A Nature Portfolio journal



https://doi.org/10.1038/s42005-025-02131-z

Directed swarm assembly due to mixed misaligned perception-dependent motility

Check for updates

Rodrigo Saavedra

& Marisol Ripoll

Biological entities as diverse as birds or bacteria frequently self-assemble to display sophisticated collective dynamical behaviors. To understand and design interactions between the individual entities that originate the different flocking behaviors is one of the current most significant challenges in active matter. Here we show how a mixture of particles with perception-dependent motility and opposite misaligned visual perception spontaneously organizes into a self-propelling bean-shaped cluster. The two species initially rotate in opposite directions which, together with the steric interactions, make them segregate into two main counter-rotating domains forming a cohesive and persistently propelling single cluster. Mixtures of particles with misaligned perception and discontinuous motility are therefore a promising pathway for the design of programmable active matter.

Interacting active agents can self-organize leading to spectacular collective behavior, e.g. at the macroscopic level in schools of fish¹, flocks of birds², and swarms of insects³. Self-organization is also observed at the microscopic level in living organisms like bacteria⁴, and active biopolymers⁵. Inspired on biology, there is a growing interest in artificially engineered systems of activated constituents, e.g. light-activated colloidal suspensions^{6–8}, driven magnetic colloids^{9–11}, or micro-robots^{12–17}. The processing of environmental information plays an essential role in the emergence of multiple collective states, such as herds of sheep¹⁸, or schools of fish¹⁹. To understand the interactions that lead to the different flocking states is one of the current most significant challenges in active matter^{20,21}. Currently, this has led to the development of the so-called programmable active matter^{22–24}, which aims to engineer systems of active automatons with adaptable collective states.

Quorum sensing is a key mechanism by which agents sense and react to environmental information. Here, some of the system constitutive agents perceive their local surroundings and then switch an intrinsic property, such as their individual motility, when a certain condition is fulfilled. As an example, certain populations of bacteria like Aliivibrio fischerei²⁵ fluoresce altogether after a chemical density threshold is surpassed. For synthetic microswimmers this has also been experimentally realized for externally controlled colloidal suspensions, where a narrow laser beam locally activates colloids according to a computer assisted feedback mechanism accounting for the local density perception, showing the particle aggregation into a circular cluster²⁶. Quorum sensing considers therefore an isotropic perception of the agents. Nonreciprocity can be also taken into account by the restriction of the perception to that occurring inside a well-defined vision cone. This has shown to lead to a plethora of collective behaviors that do not occur when interactions are reciprocal. For example, active particles with visual perception aligning their orientation based on the position of other neighboring particles, have shown to aggregate into clusters, polar filaments, and nematic bands²⁷⁻³⁰, as has been demonstrated in particle-based numerical simulations. In experiments, visual perception has also shown to generate vortical structures when imposing a local torque to light-activated colloids³¹.

A different framework in which flocking has shown to emerge is for cases combining motility with another local interaction, such as steric forces or aligning torques. In recent years, mixtures of particles displaying motility-induced self-organization into directed swarms have been investigated for mixtures of active and passive Brownian particles forming propagating interfaces³², for colloids with non-reciprocal phoretic interactions aggregating into a motile species-separated structure resembling a macroscopic Janus colloid³³, as well as for light-activated colloids with aligning interactions that form an arrow-like swarm escaping from a predator³⁴. In single-species systems, motility-induced flocking has been found in systems of self-propelled rods³⁵, as well as in systems of active particles with attractions³⁶.

In this study, we propose an experimentally feasible mechanism by which particles sedimented on a surface self-assemble into a single swarming cluster. Two types of active particles with perception displaced left or right from the motion directions are considered. Each particle type initially shows an effective rotation around the cluster center with clock or anti-clockwise directions depending on their misalignment. These rotations, together with the effect of steric interactions, trigger the assembly of a cohesive bean-shaped cluster with two counter-rotating lobes, each rich in one of the particle types, leading to the persistent motion of the cluster. We describe the procedure that leads to the emergence of this phenomena considering the individual particle behavior and then characterize it in terms of the misalignment angle and the cluster size.

Methods

We consider a system in two dimensions composed of N particles characterized by their position r_p and propulsion orientation,

Theoretical Physics of Living Matter, Institute for Advanced Simulation, Forschungszentrum Jülich, 52425 Jülich, Germany. 🖂 e-mail: m.ripoll@fz-juelich.de

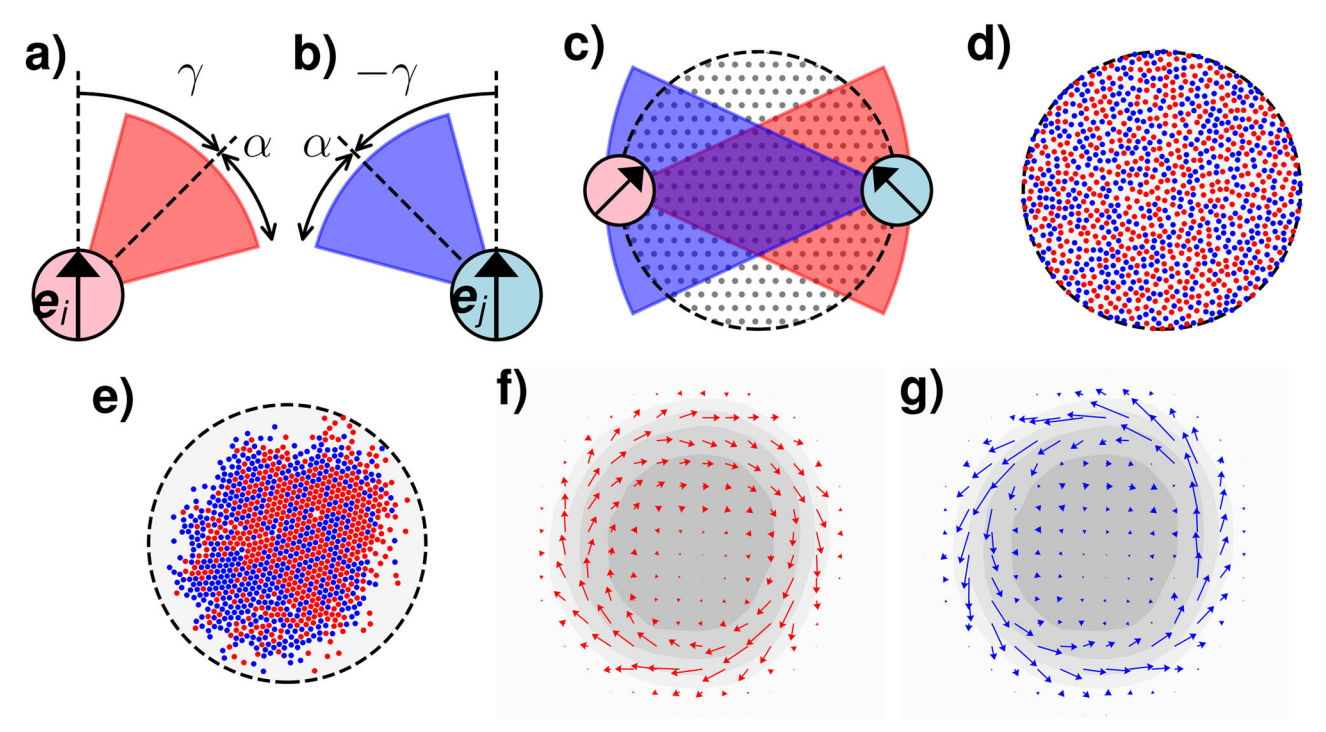


Fig. 1 | **Mixed misaligned perception-dependent motility. a**, **b** Sketches of active particles with oppositely misaligned visual perceptions. Propulsion occurs in the e_i , e_j directions. The vision cones half-width-angle is α , and their symmetry axes have a relative angle γ with the propulsion directions, this is the misalignment, which is oriented towards the right for the red particles in (**a**) and towards the left for the blue ones in (**b**). **c** Sketch of particles in a cluster boundary with maximum perception.

d Initial homogeneous configuration of an equimolar mixture of particles with perception-dependent motility with oppositely misaligned perceptions. **e** Initial collapsed configuration after very short time. **f**, **g** Average displacement of each particle type in the collapsed state showing the early counter-rotation of particles with right-handed misalignment in (\mathbf{f}) and left-handed in (\mathbf{g}) .

 $e_i \equiv (\cos \phi_i, \sin \phi_i)^T$, with ϕ_i the angle between the orientation and the x axis. Each particle i perceives all neighboring particles j placed inside the perception cone, via the function, $P_i = \sum_j (1/r_{ij})\Theta(r_{ij} - r_c)$, with $\Theta(x)$ the Heaviside function, r_{ij} the interparticle distance and r_c the maximum perception distance, similar to previous works^{37,38}. The cone half-width angle is α , while y is the angle between the cone's symmetry axis and the particle self-propulsion direction e_i , as illustrated in Fig. 1a. The particles dynamics is determined by overdamped Langevin dynamics,

$$\dot{\mathbf{r}}_{i} = \mathbf{v}_{i} \mathbf{e}_{i} + \mathbf{f}_{i}^{\text{EV}} + \sqrt{2D_{t}} \boldsymbol{\xi}_{i},
\dot{\boldsymbol{\phi}}_{i} = \sqrt{2D_{r}} \boldsymbol{\eta}_{i},$$
(1)

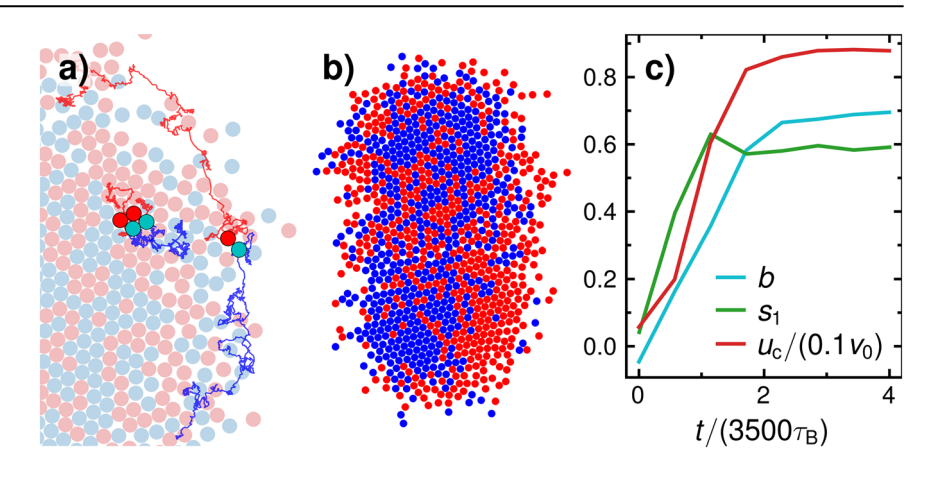
where, ξ_i and η_i are translational and orientational white noises, and D_t and D_r the translational and rotational diffusion coefficients. The excluded volume force is $f^{\text{EV}} = -\nabla U$, with $U(\sigma, \epsilon)$ the Weeks-Chandler-Anderson potential, with σ the particle diameter, and $\epsilon = 100k_{\rm B}T$ the repulsion strength. The perception-dependent particle velocity is defined by $v_i = v_0 \Theta(q_i - q^*)$, with v_0 a constant self-propulsion velocity, and $q^* =$ P_i^*/P_0 with P_i^* the threshold perception value, and a constant normalization factor $P_0 = \alpha \rho_0 R_0$ dependent on the system parameters, $\rho_0 = N/(\pi R_0^2)$ the system number density, and $R_0 = 2r_c$ also typically the initial cluster radius. This means that only particles with a large enough number of neighbors in their vision cone will become active. This mechanism induces cluster cohesion, which collectively rotate when the propulsion direction and cone direction are misaligned, this is for $y \neq 0^{38}$. Due to the intrinsic cohesion of the system, open boundary conditions are considered. The Euler algorithm is used to integrate Eq. (1) with $\Delta t = 10^{-5}$, and all quantities are normalized or expressed in simulation units, here σ and D_t . Systems with $v_0 = 40$, $D_r = 8.3$, $\rho_0 = 0.51$, $k_B T = 1$, and $\alpha = \pi/4$ are here studied, corresponding to a Péclet number Pe = 4.8, with $Pe = v_0/(\sigma D_r)$. We use $y = \pi/4$ and N = 1000unless otherwise specified. Experimentally, colloids with perceptiondependent motility have already been realized by coupling computerassisted particle tracking together with localized laser heating³⁷. This procedure is accounted by an external computer performing the choice of motility, such that to extend it to a different rule considering misaligned perception and two particle types should be straightforward.

Results

An equimolar mixture of particles is here considered, which are identical except the misalignment of their vision cones, see Fig. 1a, b. This means that to become active particles each of species need to have opposite orientation relative to the cluster center, see Fig. 1c. Simulations start from an homogeneous distribution in a circular area of radius R_0 , as shown in Fig. 1d. At first, particles with some orientation towards the cluster center become active, such that the system shows a fast initial collapse into a compact homogeneous structure as shown in Fig. 1e. In this configuration, particles in the cluster center are mainly active due to their large perception, although their actual motion is blocked due to steric interactions. Density in the external cluster layer is lower and colloids become active only if they are cooriented with their intrinsic misalignment. This means that right-misaligned particles tend to rotate around the whole cluster with a clockwise direction, and conversely left-misaligned particles, as clearly shown in Fig. 1f, g.

Particles in the external cluster layer change their properties by rotational diffusion or by colliding with other particles, specially counterrotating particles. When the new position and orientation perceive not enough neighbors, the particle remains passive until the next reorientation, which occurs when the particle has not moved significantly far away from the cluster. When the new position and orientation perceive enough neighbors, the particle might move together with another one of the same type, away from a particle of those of the other type, or get stalled in a jammed configuration, see Fig. 2a. On average, this already favors segregation by particle-type. In this way, small domains form and grow within the

Fig. 2 | Self-assembly mechanism. a, b Early separation snapshot where small red and blue (right and left misaligned perceptions) domains start to differentiate: a partial snapshots with trajectories of a few tagged particles, illustrating particle collision and initial self-sorting procedure; b complete cluster showing the initial elongation. c Time evolution of the separation parameter b, the polar order of the active particles s_1 and the cluster center of mass velocity u_c . The initial homogeneous, non-polar and static configuration shows to reach a steady separated, actively polar, and self-propelled conformation. Time is normalized by half-separation time which shows to be $3500\tau_B$, with τ_B the single particle ballistic time, and v_0 is the single particle selfpropulsion velocity.



cluster where one particle type is more frequent than the other. The domain formation on the cluster edge perturbs the rotation of particles of opposite type. This spontaneously breaks down the spatial cluster symmetry and results into an elongation of the cluster, as can be seen in Fig. 2b. With the increase of the average domains size, the average cluster alignment produces also larger rearrangements in neighboring domains reaching the cluster center, with the eventual formation of short-lived dislocations, which enhance the domains rearrangement and growth, see Supplementary Movie 1. When the domains are large enough they start to rotate in the direction of the domainant particle type.

In order to quantitatively characterize the self-sorting procedure, we consider three quantities. First, we define the separation parameter b, as a useful alternative to the standard Moran's index^{39,40}. To compute this parameter, we consider as neighboring particles those that are separated by a small distance of $r=2\sigma$. For each particle j, we count the number of neighbors of the same type $n_{j,s}$ (these are left for a left particle, or conversely right for a right particle), the number of neighbors of the opposite type $n_{j,o}$ (right for a left particle), and we average and normalize by the total number of neighbors as

$$b = \frac{1}{N} \sum_{i=1}^{N} \frac{n_{j,s} - n_{j,o}}{n_{j,s} + n_{j,o}}.$$
 (2)

With this definition, the separation parameter varies from b=0 for perfectly homogeneous configurations, to b=1 for perfect separation without any interface, such that in between values are obtained when one particle type rich subdomains form. The time increase of b displayed in Fig. 2c, shows an initially homogeneous configuration which progressively separates, reaching a steady state value at longer times. At long times, the separation value saturates in a steady state value, which for the standard model parameters here employed is $b\simeq 0.7$. Time is normalized with the time at which the cluster velocity has reached half the saturation value, which for the standard parameters here used is roughly $\tau_{\rm s}\simeq 3500\tau_{\rm B}$, with $\tau_{\rm B}=\sigma/\nu_0$ the single particle ballistic time.

We also compute the overall polar order of the particles displacements s_1 , defined as

$$s_1(t) = \left| \frac{1}{N} \sum_{i=1}^{N} e^{i\theta_i(t)} \right|,\tag{3}$$

where θ_i corresponds to the polar angle of the particle normalized effective velocity $\hat{v}_i = v_i/v_i$, and $v_i = \Delta r_i/\Delta t$ is calculated from the particle displacements. This polarity is an intrinsic cluster property, such that needs to be calculated in the centre of mass reference, which is ensured by considering time intervals in which the cluster center of mass has essentially not

moved, here $\Delta t = 20\tau_{\rm B}$. Polar order increases similar to b saturating to a persistent value, as shown in Fig. 2c. Similarly to the case of single component clusters³⁸, there is no overall alignment of the particles actual orientation since the polar order relates to the particle displacements, which occurs all in the same direction.

The large polarity of the active particles has as a consequence the overall motion of the cluster. Assuming a ballistic self-propulsion, the displacements on the main polar direction of the cluster center of mass need to be evaluated in larger time intervals, here $\Delta t = 400\tau_B$, and then averaged over 10 realizations, such that a time dependent velocity u_c is computed, see Fig. 2c. This averaged velocity starts from a vanishing value in the initial nonseparated state, and increases until a constant velocity which, for our parameters, is 9% of the velocity of a single active colloid, v_0 . Separation parameter, induced polarity and cluster velocity are therefore strongly interconnected. The time evolution of the three quantities towards the steady state is not completely simultaneous, as shown in Fig. 2c. Maximum polarity is first achieved in the cluster reference frame and the maximum value of the cluster center of mass velocity requires slightly longer times. The separation parameter grows simultaneously to the polarity, but continues increasing after the maximum orientation is achieved, such that is the last quantity to reach steady-state.

When the maximum separation is reached, the cluster organizes in two main domains of typically the same size. Each domain is composed by mainly one particle type, as shown in Fig. 3a, and each of them rotates according to the misalignment of the majority, as shown in Fig. 3b. The high perception in the cluster center makes that many more particles are active than in the outside of the cluster. The two counter-rotating domains remain completely adhered to each other, and given the difference in density, the particles at the center move much slower than those in the external cluster layer. This also makes that the two stagnation points are not central to the respective domains, but are placed closer to the cluster center, see Fig. 3b. Active particles at the outside part of the cluster drag all other particles along the corresponding rotation, regardless if they are active or passive, or even of the opposite particle type. The cluster polar order, self-propulsion direction and overall cluster motion are therefore determined by the few active particles placed at the outside cluster shell. These few particles remain active and shortly accumulate when arriving to the symmetry axis where the two counter-rotating domains join. This accumulation occurs only in one of the sides of the symmetry axis deforming the cluster shape from elongated to a bean shape, with the convex side in the motion direction, see Fig. 3b. The trajectory of a few tagged particles is presented in Fig. 3c in the laboratory reference frame, see also Supplementary Movie 2. The displayed motion shows to be clearly periodic showing how each particle rotates within one of the domains and how the cluster propels in a well defined direction for a long period of time.

The phenomena as above described is then a consequence of the ordered collisions between particles, such that the presence of steric interactions seems central for the self-assembly of the directed swarm. In order to

Fig. 3 | Structure and swarming mechanism of the steady state clusters. a, b Snapshots of the cluster in a steady state, where the two counter-rotating domains can be distinguished, with red and blue particles indicating intrinsic right and left misaligned perceptions. In (a) dark (light) colors correspond to active (passive) particles, in (b) arrows depict the direction and speed of the particle displacements, in the cluster center of mass reference frame. c Trajectories of a few particles within the cluster, showing the overall cluster displacement. Color bar indicates time evolution, and the small snapshots illustrate the corresponding cluster states. With τ_B the single particle ballistic time.

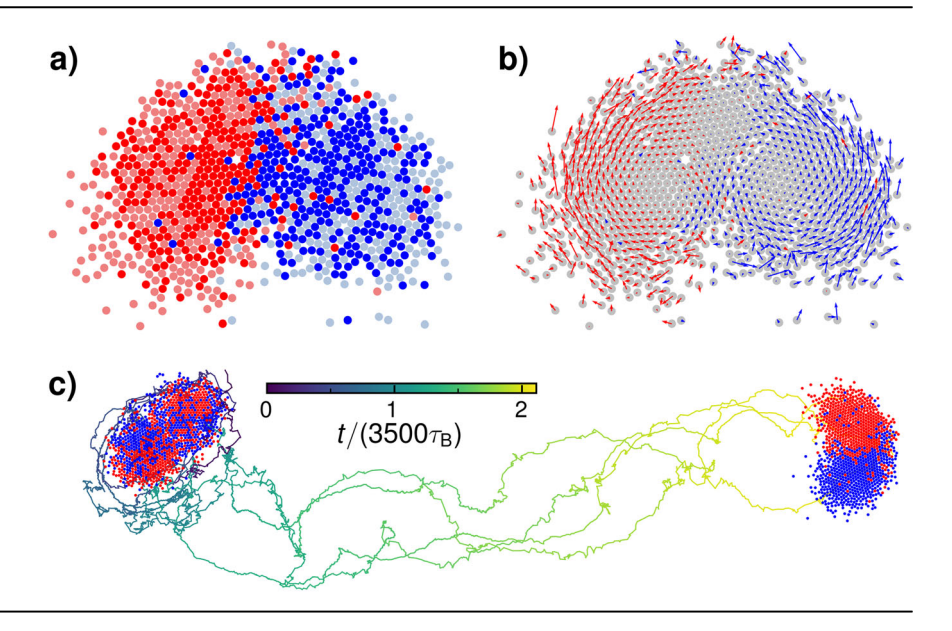
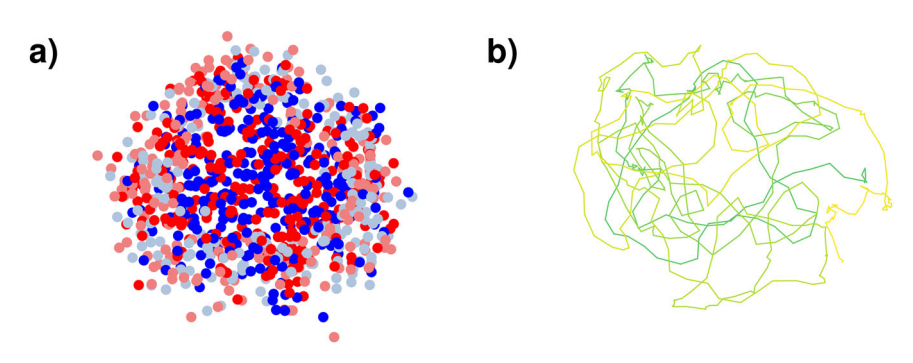


Fig. 4 | Importance of steric interactions.

a Snapshot and (b) tagged particles trajectories of a cluster in which particles have no excluded volume interactions, showing that these are crucial for the described particle segregation and overall cluster self-propulsion. In (a) red and blue particles indicate particles with intrinsic right and left misaligned perceptions and dark (light) colors correspond active (passive) particles. The color gradient in (b) indicates time evolution as in Fig. 3c.



verify the extent of how crucial steric interactions are, we perform some simulations in which the excluded volume between particles is switched off, this is considering the interaction of ideal point particles. An snapshot of a late conformation of a cluster and one particle trajectory is presented in Fig. 4a. The perception-dependent motility mechanism shows to keep the particles as a cohesive cluster, but there is no indication of separation into domains of different particle types and also no cluster self-propulsion, as can be seen in the trajectory of Fig. 4b. The misalignment still makes that the two populations rotate in opposite directions similar as Fig. 1f, g, this resulting in no net sorting or motion.

Our discussion until now has just considered a fixed set of parameters, which result into a stable solid behavior, as well as a particular value of the steady state value of the cluster velocity u_{c} motion persistence, or characteristic self-assembly times. In order to better understand the system behavior, we investigate now the influence of the misalignment angle y. In the limit of very small values of y, none of the components are expected to induce swirling, and since particle are basically identical interactions no separation is possible. On the other limit, a misalignment close to $\pi/2$ is not even able to keep the cohesion of the cluster in the case of single component clusters³⁸, such that no assembly occurs either. Results in Fig. 5a show the increase of the steady state velocity with y, as well as a speed up of the procedure, for a certain range of misalignment values. In Fig. 5b, the measured steady-state velocities \overline{u}_c , show to be non-vanishing only in the interval $0.2 \le y/\pi \le 0.3$, and also that within this interval the increase of \overline{u}_c is approximately linear. The measured characteristic self-assembly times t_s are shown in Fig. 5c, conversely show a linearly decrease with γ , within the same interval as the \overline{u}_c . For misalignment outside this range, swirling is observed in single component systems but the self-sorting procedure is not strong enlough in comparison to the related fluctuations to result into the assembly of a coherent swarming cluster.

In the framework of possible applications is also important to discern how many particles are necessary to observe the cluster self-assembly and swarming. In the limit of very small clusters, excluded volume interactions between particles are not significant enough to result in the sorting procedure, which is easy to understand for clusters from 2 to 20 particles for which only counter rotation is to be expected. We perform further simulations for clusters from 100 to 2000 particles, and a summary of results is shown in Fig. 6. Clusters more than 300 particles show the behavior discussed until now for 1000 particles, this is with a self-sorting of the particles in two counter-rotating domains, as can be seen in Fig. 6a, b. For smaller clusters the self-sorting is not persistent and the cluster constantly oscillates in between states, in some states the particles have a large sorting degree (see Fig. 6c) and the cluster shows self-propulsion. In other states particles are almost homogeneously distributed and the cluster performs only a Brownian motion. This results in a much smaller, but still significant, value of the cluster center of mass velocity. For a comparison of the purely Brownian motion of a cluster with no misalignment, and the enhanced Brownian motion of a cluster with 100 particles with mixed misaligned perceptiondependent motility particles see Supplementary Movie 3. The time evolution of the cluster center of mass velocity is shown in Fig. 6d for clusters with four different sizes. The steady state cluster velocity \overline{u}_c shows to generally increase with cluster size N, together with the characteristic time t_s to reach such state. The explicit dependence of \overline{u}_c with N in Fig. 6e shows an approximately linear growth with N for small clusters and a saturation of this value from approximately N = 400. For small clusters, the velocity increases since for more states with sorted domains are expected with

Fig. 5 | Misalignment angle dependence of the cluster swarming properties. a Time evolution of the cluster center of mass velocity u_c for systems with varying misalignment angle γ . b Steady state values of the cluster velocity \overline{u}_c , and c characteristic time to reach the steady state t_s . Grey lines in (\mathbf{b}, \mathbf{c}) are a guide to eye, τ_B is the single particle ballistic time and ν_0 the single particle self-propulsion velocity.

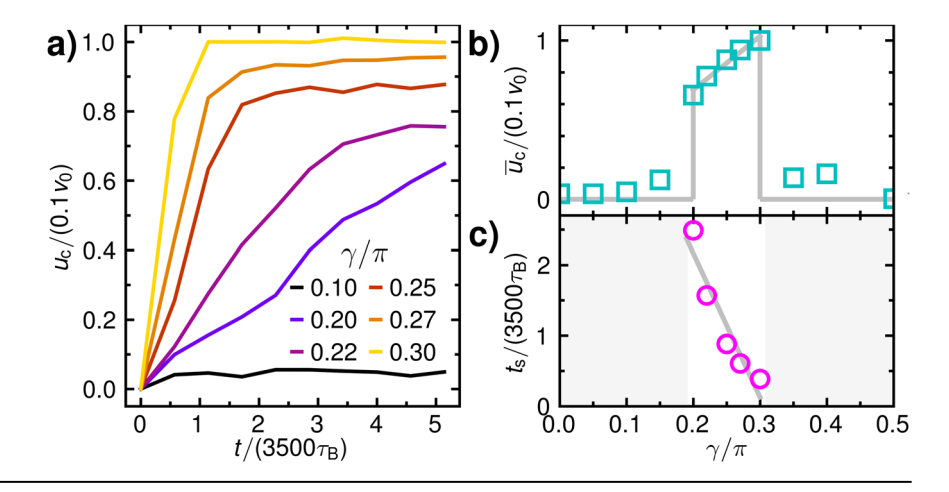
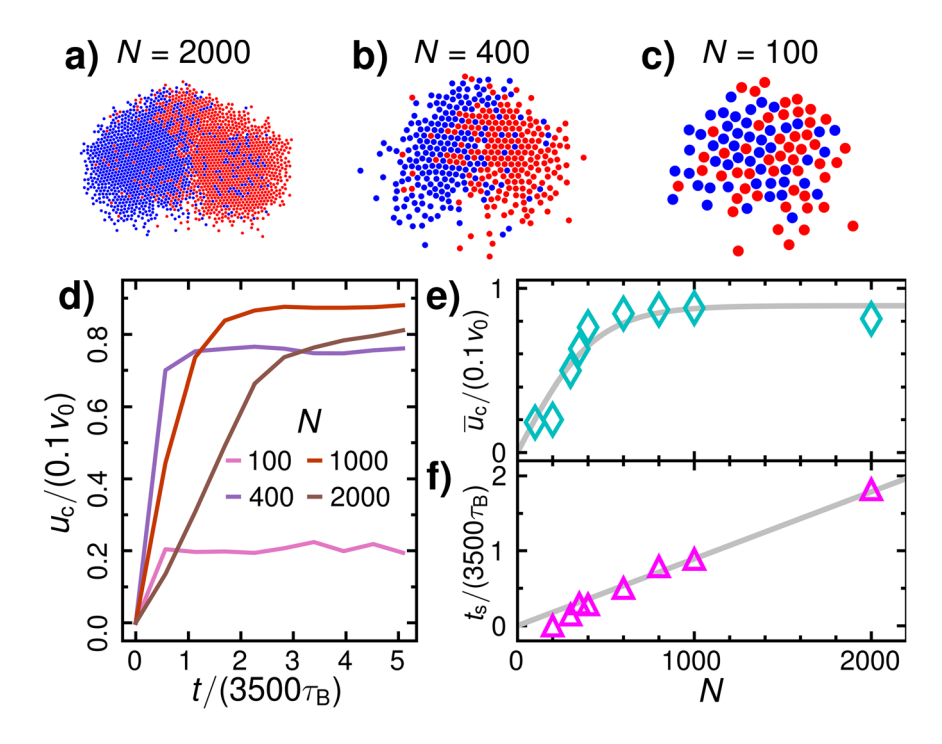


Fig. 6 | Cluster size dependence of the cluster swarming properties. a–c Snapshots steady state clusters with different number of particles, where red and blue particles indicate intrinsic right and left misaligned perceptions. d Time evolution of the cluster center of mass velocity $u_{\rm c}$ for systems with varying number of total particles N. e Steady state values of the cluster velocity $\overline{u}_{\rm c}$, and f characteristic time to reach the steady state $t_{\rm s}$. Grey lines in (e, f) are a guide to eye, $\tau_{\rm B}$ is the single particle ballistic time and $\nu_{\rm 0}$ the singe particle self-propulsion velocity.



increasing number of particles. Meanwhile, for clusters with two steady domains, the velocity is determined by the angular velocity of the counterrotations. On the other hand, the time necessary to reach the steady state linearly grows with the number of particles, which can be understood since the collision frequency does not change, but the number of collisions necessary for the sorting clearly increases with the number of particles.

Various other parameters are expected to have a significant influence on the cluster behavior, such as the width of the vision cone α , the perception range $r_{\rm c}$ or threshold q^* or the number of considered particles. Similarly, the behavior of the cluster will vary for the cases of non-equimolar or non-symmetric mixtures. Besides the main swarming properties, namely cluster velocity $u_{\rm c}$ persistence, and characteristic self-assembly time, we surmise that the stability, or the type of trajectories are also largely affected. These dependencies are currently under investigation and will be subject of a forthcoming publication.

Conclusions

We have here introduced a swarming mechanism which emerges when considering a group of particles with an initially homogeneous mixture of particles with oppositely misaligned perception-dependent motility. Collisions between particles with opposite misalignment originate a self-organized sorting procedure such that the cluster remains cohesive and persistently propagates. The resulting cluster is elongated and organized in two main counter-rotating subdomains and the overall motion is then driven by the overall alignment of the active particles velocities. Stable counter-rotation of the two main domains occurs for a well-determined interval of misalignment for clusters larger than 300 particles. For smaller clusters the domains are not stable, although the clusters still display a significant self-propulsion. The mechanism here described is completely different to previous studies, since due to the misaligned perception-dependent motility, it does not require of any explicit particle alignment, nor external torques, or forces, it being still able to result into a motion in well defined angular and linear momentums. The swarming strategy can be implemented in different types of experiments such as colloids activated by light or in robot ensembles, serving then various potential purposes.

Data availability

The data that support the findings of this study are available from the corresponding authors upon reasonable request. Numerical source data for graphs can be now found at: https://doi.org/10.6084/m9.figshare.28844078.

Code availability

The custom code for the simulations is available from the corresponding authors upon reasonable request.

Received: 6 December 2024; Accepted: 7 May 2025; Published online: 17 May 2025

References

- Tunstrøm, K. et al. Collective states, multistability and transitional behavior in schooling fish. PLoS Comput. Biol. 9, e1002915 (2013).
- Ballerini, M. et al. Interaction ruling animal collective behavior depends on topological rather than metric distance: evidence from a field study. Proc. Natl. Acad. Sci. USA 105, 1232–1237 (2008).
- Attanasi, A. et al. Collective behaviour without collective order in wild swarms of midges. PLoS Comput. Biol. 10, e1003697 (2014).
- Aranson, I. S. Bacterial active matter. Rep. Prog. Phys. 85, 076601 (2022).
- Koenderink, G. H. et al. An active biopolymer network controlled by molecular motors. *Proc. Natl. Acad. Sci. USA* 106, 15192–15197 (2009)
- Vutukuri, H. R., Lisicki, M., Lauga, E. & Vermant, J. Light-switchable propulsion of active particles with reversible interactions. *Nat. Commun.* 11, 2628 (2020).
- Gomez-Solano, J. R., Roy, S., Araki, T., Dietrich, S. & Maciołek, A. Transient coarsening and the motility of optically heated Janus colloids in a binary liquid mixture. Soft Matter 16, 8359–8371 (2020).
- Zhang, B., Sokolov, A. & Snezhko, A. Reconfigurable emergent patterns in active chiral fluids. *Nat. Commun.* 11, 4401 (2020).
- Bricard, A. et al. Emergent vortices in populations of colloidal rollers. Nat. Commun. 6, 7470 (2015).
- Kawai, T., Matsunaga, D., Meng, F., Yeomans, J. M. & Golestanian, R. Degenerate states, emergent dynamics and fluid mixing by magnetic rotors. Soft Matter 16, 6484–6492 (2020).
- 11. Junot, G., Cebers, A. & Tierno, P. Collective hydrodynamic transport of magnetic microrollers. *Soft Matter* **17**, 8605–8611 (2021).
- Yu, J., Yang, L. & Zhang, L. Pattern generation and motion control of a vortex-like paramagnetic nanoparticle swarm. *Int. J. Robot. Res.* 37, 912–930 (2018).
- 13. Xie, H. et al. Reconfigurable magnetic microrobot swarm: multimode transformation, locomotion, and manipulation. *Sci. Robot.* 4https://doi.org/10.1126/scirobotics.aav8006 (2019).
- Dorigo, M., Theraulaz, G. & Trianni, V. Swarm robotics: past, present, and future [Point of View]. Proc. IEEE 109, 1152–1165 (2021).
- Hussein, H. et al. Actuation of mobile microbots: a review. Adv. Intell. Syst. n/a, 2300168 (2023).
- Yu, Z. et al. Swarming magnetic photonic-crystal microrobots with on-the-fly visual pH detection and self-regulated drug delivery. *InfoMat* n/a, e12464 (2023).
- 17. Hou, Y. et al. A review on microrobots driven by optical and magnetic fields. *Lab Chip* **23**, 848–868 (2023).
- Gómez-Nava, L., Bon, R. & Peruani, F. Intermittent collective motion in sheep results from alternating the role of leader and follower. *Nat. Phys.* 18, 1–8 (2022).
- Wang, W. et al. The impact of individual perceptual and cognitive factors on collective states in a data-driven fish school model. *PLoS Comput. Biol.* 18, e1009437 (2022).
- 20. Gompper, G. et al. The 2020 motile active matter roadmap. *J. Phys.: Condens. Matter* **32**, 193001 (2020).
- Abaurrea Velasco, C., Abkenar, M., Gompper, G. & Auth, T. Collective behavior of self-propelled rods with quorum sensing. *Phys. Rev. E* 98, 022605 (2018).
- 22. Wang, W., Giltinan, J., Zakharchenko, S. & Sitti, M. Dynamic and programmable self-assembly of micro-rafts at the air-water interface. *Sci. Adv.* 3, e1602522 (2017).

- Nava, L. G., Großmann, R., Hintsche, M., Beta, C. & Peruani, F. A novel approach to chemotaxis: active particles guided by internal clocks. EPL 130. 68002 (2020).
- Ceron, S., Gardi, G., Petersen, K. & Sitti, M. Programmable selforganization of heterogeneous microrobot collectives. *Proc. Natl. Acad. Sci. USA* 120, e2221913120 (2023).
- Stevens, A. M. & Greenberg, E. P. Quorum sensing in vibrio fischeri: essential elements for activation of the luminescence genes. *J. Bacteriol.* 179, 557–562 (1997).
- Bäuerle, T., Fischer, A., Speck, T. & Bechinger, C. Self-organization of active particles by quorum sensing rules. *Nat. Commun.* 9, 3232 (2018).
- 27. Barberis, L. & Peruani, F. Large-scale patterns in a minimal cognitive flocking model: incidental leaders, nematic patterns, and aggregates. *Phys. Rev. Lett.* **117**, 248001 (2016).
- Costanzo, A. Milling-induction and milling-destruction in a Vicsek-like binary-mixture model. EPL 125, 20008 (2019).
- Negi, R. S., Winkler, R. G. & Gompper, G. Emergent collective behavior of active Brownian particles with visual perception. Soft Matter 18, 6167–6178 (2022).
- Negi, R. S., Winkler, R. G. & Gompper, G. Collective behavior of selfsteering active particles with velocity alignment and visual perception. *Phys. Rev. Res.* 6, 013118 (2024).
- Bäuerle, T., Löffler, R. C. & Bechinger, C. Formation of stable and responsive collective states in suspensions of active colloids. *Nat. Commun.* 11, 2547 (2020).
- Wysocki, A., Winkler, R. G. & Gompper, G. Propagating interfaces in mixtures of active and passive Brownian particles. *N. J. Phys.* 18, 123030 (2016).
- Agudo-Canalejo, J. & Golestanian, R. Active phase separation in mixtures of chemically interacting particles. *Phys. Rev. Lett.* 123, 018101 (2019).
- 34. Chen, C.-J. & Bechinger, C. Collective response of microrobotic swarms to external threats. *N. J. Phys.* **24**, 033001 (2022).
- Bär, M., Großmann, R., Heidenreich, S. & Peruani, F. Self-propelled rods: insights and perspectives for active matter. *Annu. Rev. Condens. Matter Phys.* 11, 441–466 (2020).
- Caprini, L. & Löwen, H. Flocking without alignment interactions in attractive active brownian particles. *Phys. Rev. Lett.* 130, 148202 (2023).
- Lavergne, F. A., Wendehenne, H., Bäuerle, T. & Bechinger, C. Group formation and cohesion of active particles with visual perception-dependent motility. Science 364, 70–74 (2019).
- Saavedra, R., Gompper, G. & Ripoll, M. Swirling due to misaligned perception-dependent motility. Phys. Rev. Lett. 132, 268301 (2024).
- 39. Moran, P. Notes on continuous stochastic phenomena. *Biometrika* **37**, 17–23 (1950).
- Dirk, R., Fischer, J. L., Schardt, S., Ankenbrand, M. J. & Fischer, S. C. Recognition and reconstruction of cell differentiation patterns with deep learning. *PLoS Comput. Biol.* 19, e1011582 (2023).
- 41. Centre, J. S. J. large-scale Res. facilities 7, A182 (2018).

Acknowledgements

This work was financially supported by the CONACyT-DAAD scholarship program. We gratefully acknowledge the computing time granted by the JARA Vergabegremium and provided on the JARA Partition part of the supercomputer JURECA at Forschungszentrum Jülich⁴¹.

Author contributions

R.S. and M.R. designed the investigation and discussed the results. R.S. wrote the simulation code and conducted the numerical simulations. M.R. wrote the manuscript. R.S. and M.R. finalised and approved the manuscript.

Funding

Open Access funding enabled and organized by Projekt DEAL.

Competing interests

The authors declare no competing interests.

Additional information

Supplementary information The online version contains supplementary material available at https://doi.org/10.1038/s42005-025-02131-z.

Correspondence and requests for materials should be addressed to Marisol Ripoll.

Peer review information *Communications Physics* thanks Jaideep Katuri and the other, anonymous, reviewer(s) for their contribution to the peer review of this work. A peer review file is available.

Reprints and permissions information is available at http://www.nature.com/reprints

Publisher's note Springer Nature remains neutral with regard to jurisdictional claims in published maps and institutional affiliations.

Open Access This article is licensed under a Creative Commons Attribution 4.0 International License, which permits use, sharing, adaptation, distribution and reproduction in any medium or format, as long as you give appropriate credit to the original author(s) and the source, provide a link to the Creative Commons licence, and indicate if changes were made. The images or other third party material in this article are included in the article's Creative Commons licence, unless indicated otherwise in a credit line to the material. If material is not included in the article's Creative Commons licence and your intended use is not permitted by statutory regulation or exceeds the permitted use, you will need to obtain permission directly from the copyright holder. To view a copy of this licence, visit http://creativecommons.org/licenses/by/4.0/.

© The Author(s) 2025